Engineering of microstructures of protonic ceramics by a novel rapid laser reactive sintering for ceramic energy conversion devices

Shenglong Mu[a], Zeyu Zhao[a], Jincheng Lei[b], Yuzhe Hong[a], Tao Hong[a], Dong Jiang[a], Yang Song[b], William Jackson[a], Kyle S. Brinkman[a], Fei Peng[a], Hai Xiao[b], Jianhua Tong[a],*

[a] Department of Materials Science and Engineering, Clemson University, SC 29634, USA
[b] Department of Electrical and Computer Engineering, Clemson University, SC 29634, USA

A B S T R A C T

The solid state reactive sintering (SSRS) characteristic with the assistance of sintering aids (e.g., NiO) has been proven to be an effective method for achieving high-quality proton conducting oxide electrolytes at relatively low sintering temperatures (e.g., < 1400 °C). In this work, instead of performing a long-term (e.g., > 10 h) SSRS in a conventional high-temperature furnace, a novel rapid laser heating process was used to perform SSRS, which was named as rapid laser reactive sintering (RLRS). This RLRS method was confirmed to be able to sinter protonic ceramics with well-engineered microstructures within a short time (e.g., < 10 s). Using the proton conducting oxides of $BaCe_{0.7}Zr_{0.1}Y_{0.1}Yb_{0.1}O_{3-\delta}$ (BCZYYb) and $BaZr_{0.8}Y_{0.2}O_{3-\delta}$ (BZY20) as case study, the crack-free protonic ceramic parts of straight strips (~10 mm in length, ~1 mm in width, and 30–200 μm in thickness), spiral strips (~200 mm in length, ~1 mm in width, and 30–200 μm in thickness), and squared films (~4.5 mm in both length and width and 30–200 μm in thickness) were successfully fabricated by RLRS method. The sintered parts usually showed fully dense large-grained and highly porous regions, which can potentially serve as electrolytes and electrode scaffolds for single cells or half-cells. The X-ray diffraction results indicated that the pure perovskite structures were obtained for both BCZYYb and BZY20 by RLRS from inexpensive carbonates and single metal oxides. The preliminary electrochemical impedance measurement for the dense strips after removal of porous regions by picosecond laser machining showed a reasonable in-plane protonic conductivities. This new RLRS method demonstrated the feasibility and promise of the rapid additive manufacturing of hierarchical ceramic energy conversion devices.

1. Introduction

Proton conducting oxides (i.e., protonic ceramics) possess low transport activation energies which allow for high ionic conductivity at low operating temperatures (250–600 °C) [1–4]. The protonic ceramic energy devices such as protonic ceramic fuel cells (PCFCs) [3–8], protonic ceramic electrolysis cells (PCECs) [9,10] solid state ammonia synthesis cells [11,12], hydrogen or water sensors [13,14], steam permeable membrane reactors [15,16], and hydrogen permeable membrane reactors [17–19], have been intensively studied. However, because of the high refractory nature of the materials, state-of-the-art proton conducting oxides of yttrium-doped barium zirconates and cerates usually require sintering temperatures higher than 1700 °C to achieve acceptable relative densities [1,2]. The high-temperature requirements make it very difficult to fabricate ceramic energy devices based on dense protonic ceramic electrolytes. On the other hand, the proton conducting oxides also need to be fabricated into highly porous nanostructures as electrode scaffolds for further improving device performance (e.g., direct hydrocarbon PCFCs), which requires even lower fabrication temperatures or new techniques which can sinter protonic ceramic under a specific temperature distribution instead of the conventional co-firing technique.

Fully densified protonic ceramics were previously demonstrated by careful optimization of sintering conditions, modification of powder properties, assistance of sintering aid materials, and assistance of compressive stress from substrate, etc. [20–27]. Increasing the sintering temperature and time, while improving grain size and relative density, frequently resulted in the barium deficiency and the emergence of deleterious second phases, which inevitably cause low total conductivity [20–22]. The use of nanoparticles powders prepared via polymeric sol-gel or combustion methods provided relatively good performance [23,24], which, however, is economically unfavorable for industrial

---

* Corresponding author.
  E-mail address: jianhut@clemson.edu (J. Tong).

application. Sintering aids such as ZnO, NiO, CuO, and CoO have been added to yttrium doped barium zirconates (BZY) powders prepared by wet chemistry methods and the grain size and density of the BZY pellets have been increased to some degree [25–27]. Although the sintering mechanism is not clear, the addition of sintering aids can often decrease the sintering temperature to as low as 1350 °C, which makes it possible to prepare SOFCs by inexpensive co-fired techniques. Using the similar sintering aids, Tong et al. developed a solid state reactive sintering (SSRS) technique [28–30], which combines the solid state reaction and additive-assisted sintering into one step and allows the fabrication of dense large-grained pellets of $BaZr_{0.8}Y_{0.2}O_{3-\delta}$ from barium carbonate, yttrium oxide, and zirconium oxide at moderate firing temperatures (e.g., 1400 °C). This SSRS technique has been successfully used for fabricating PCFC button cells at moderate firing temperatures, and promising performance has been demonstrated for both power density and long-term stability [5,31]. Using the same SSRS technique, tubular protonic ceramic membrane reactors were fabricated resulting in promising performance for methane dehydroaromatization due to the simultaneous removal of hydrogen and addition of oxygen [32].

Although the SSRS technique has been recently developed and successfully applied, it still needs long-term cofiring of the electrolyte and electrode (e.g., anode cermet) at a high temperature around 1400 °C. This high temperature usually eliminates the possibility of creating nanostructures for high-performance supporting electrodes when making half-cell using the cofiring method. Furthermore, it is still a challenge to combine the PCFCs/PCECs with low-temperature and cost-effective stainless steel interconnects. Therefore, new additive manufacturing processing techniques for selectively depositing and sintering different layers of protonic ceramics for achieving controllable microstructures (e.g., fully densified and highly porous) are desperately needed to accelerate the progress of protonic ceramic energy devices further. Additive manufacturing (AM), the process of digital joining materials layer by layer based on computer-aided design (CAD) [33], allows us to produce versatile complicated configurations on demand [34]. The AM technology is one of the most promising techniques for digitally manufacturing devices composed of hierarchical multilayers including ceramic energy devices (e.g., PCFCs). However, to ensure the rapid AM process, it needs to selectively and instantaneously consolidate various ceramic precursor layers under different conditions for achieving controllable microstructures.

In this work, by combining the selective laser sintering/melting technique [35] and the solid state reactive sintering technique [26–38], we developed a new rapid laser reactive sintering technique for selectively and instantaneously processing ceramics with well-controlled microstructures (fully dense and highly porous). Using the state-of-the-art protonic ceramics $BaCe_{0.7}Zr_{0.1}Y_{0.1}Yb_{0.1}O_{3-\delta}$ (BCZYYb) and $BaZr_{0.8}Y_{0.2}O_{3-\delta}$ (BZY20) as examples, we have demonstrated the successful fabrication of dense large-grained (for electrolyte) and highly porous (for electrode scaffold) crack-free protonic ceramic parts with different configurations from inexpensive carbonates and binary oxides. The initial measurement of the transport properties of the dense BCZYYb strips showed promising protonic conductivities. This new method can be directly used for the fabrication of the micro-PCFCs, micro-PCECs, and micro electrochemical sensors based on proton conducting oxides, which usually were fabricated using a complicated combination of thin film deposition and MEMS technology [39]. Furthermore, this method can also potentially enhance the feasibility of the rapid additive manufacturing of hierarchical ceramic devices for energy conversion.

2. Experiments

2.1. Rapid laser reactive sintering

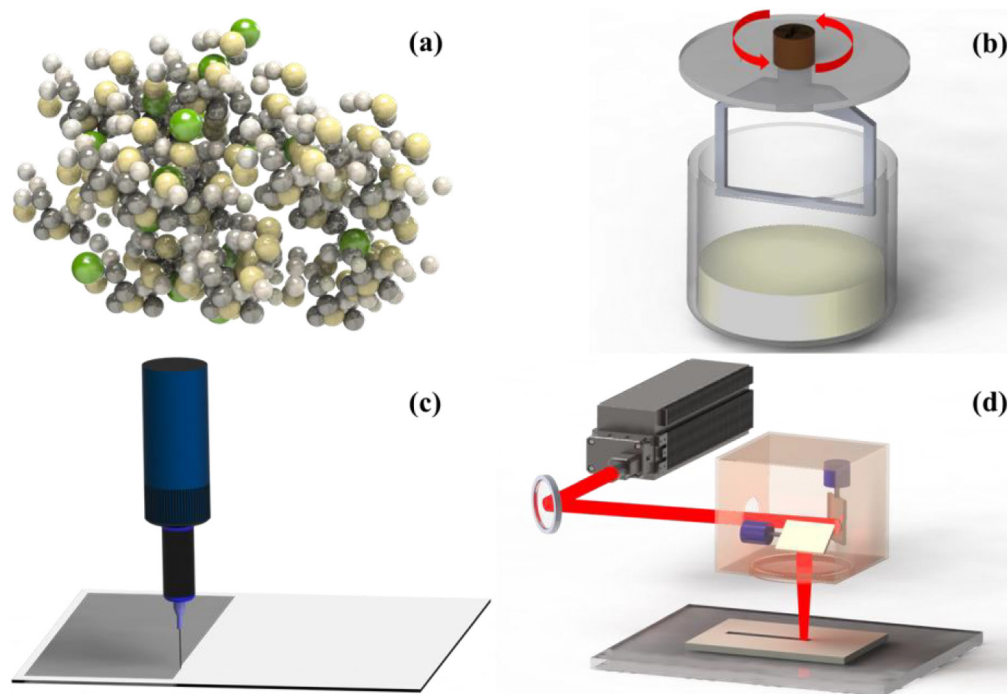Fig. 1 shows that the rapid laser reactive sintering (RLRS) of protonic ceramics can be performed through four steps. Using BCZYYb as a case study, these four steps of the RLRS are detailed as follow. a) Mix precursor solids. According to the composition of $BaCe_{0.7}Zr_{0.1}Y_{0.1}Yb_{0.1}O_{3-\delta}$, stoichiometric amounts of precursor solids of $BaCO_3$, CeO_2, ZrO_2, Y_2O_3, and Yb_2O_3 together with 1.0 wt% of NiO sintering additive (based on BCZYYb weight) were mixed by ball-milling for 48 h with isopropanol solvent and 3 mm YSZ grinding media. After drying to remove the solvent of isopropanol, the solid precursor powders were ready for paste preparation. b) Prepare precursor paste. The de-ionized water solvent and the DARVAN dispersant were added to the dry precursor powders. After ball-milling for 24 h with 3 mm YSZ grinding media, the stable slurry with the solid amount around 30–50% of total volume and the dispersant amount around 2–10 wt% of water weight was achieved. HPMC (hydroxypropyl methylcellulose) binder in the amount of 1–5 wt% of water was then added to the slurry and mechanically stirred for 20 min. After aging for 24 h, the precursor paste was ready for layer deposition. c) Deposit precursor layer. The paste was 3D printed via a micro extruder with a needle diameter of 0.5 mm. By controlling the extrusion speed and the three-dimensional movement of the stage, the paste layer with a controlled thickness was deposited on a fused silica wafer or a dense alumina plate substrates. In addition, a simple Doctor Blade was also employed to deposit the precursor layer for processing comparison. These two deposition methods for the flat green layers were confirmed to behave similarly for the purpose of RLRS in this work. d) Perform RLRS. The RLRS of the precursor layer on flat substrates was performed using a CO_2 laser beam (Firestar v20, SYNRAD, Inc., WA, USA, wavelength 10.6μm) controlled by a two-axial galvo scanner (intelliSCAN 14, SCANLAB, Germany). The paste layer thickness, the substrates, and the laser operation parameters of scan speed, power, defocus distance, spot size, and energy density were optimized for engineering the microstructures of the resulted BCZYYb ceramic parts. The ceramic parts of the proton conducting oxide of BZY20, the most refractory protonic ceramic material, were also fabricated by following the same processes employed for the fabrication of BCZYYb strips.

2.2. Characterization

The as-prepared BCZYYb and BZY20 strips were ground into fine powders and subjected to the crystal structure characterization using X-ray diffraction (XRD). A Rigaku Ultima IV diffractometer with a monochromatic Cu Kα radiation was used to record the data at a rate of 1 °/min in the range of 15–85 degree. The microstructures of the protonic ceramics were investigated by Scanning Electron Microscopy (SEM Hitachi S4800). The various strip samples prepared under different conditions with well-engineered microstructures were identified carefully using secondary electron micrographs.

2.3. Conductivity measurement

In this work, the proton conductivities for the BCZYYb ceramic strips prepared using RLRS were analyzed by electrochemical impedance spectroscopy (EIS). The symmetrical cells for EIS measurement are described in Fig. 2, which allows the in-plane conductivity measurement. The as-prepared protonic ceramic strips typically contain a dense center and two porous edges due to the Gaussian distribution of laser power. A Picosecond laser (PS-laser, APL-4000, ATTODYNE, wavelength 1064 nm, pulse width 6 ps, repetition rate 100 kHz, output power 15% of 4 W) was used remove the porous parts, leaving the fully dense region for EIS testing. In order to improve the measurement accuracy and avoid mechanical failure, five dense protonic ceramic strips with 1 mm length were embedded in pre-cut channels on a fused silica substrate. Silver paste was filled into two large troughs to obtain well-contacted electrodes. Gold wires were used to extend electrodes to the external conducting wires. The EIS data were recorded using a Gamry Reference 600 plus with a perturbation voltage of 10 mV in the frequency range of 5 mHz to 5 MHz at temperatures of 300–700 °C under

Fig. 1. Schematic description of rapid laser reactive sintering (RLRS) process. (a) Mix precursor solids, (b) prepare precursor paste, (c) deposit precursor layer, and (d) perform RLRS.
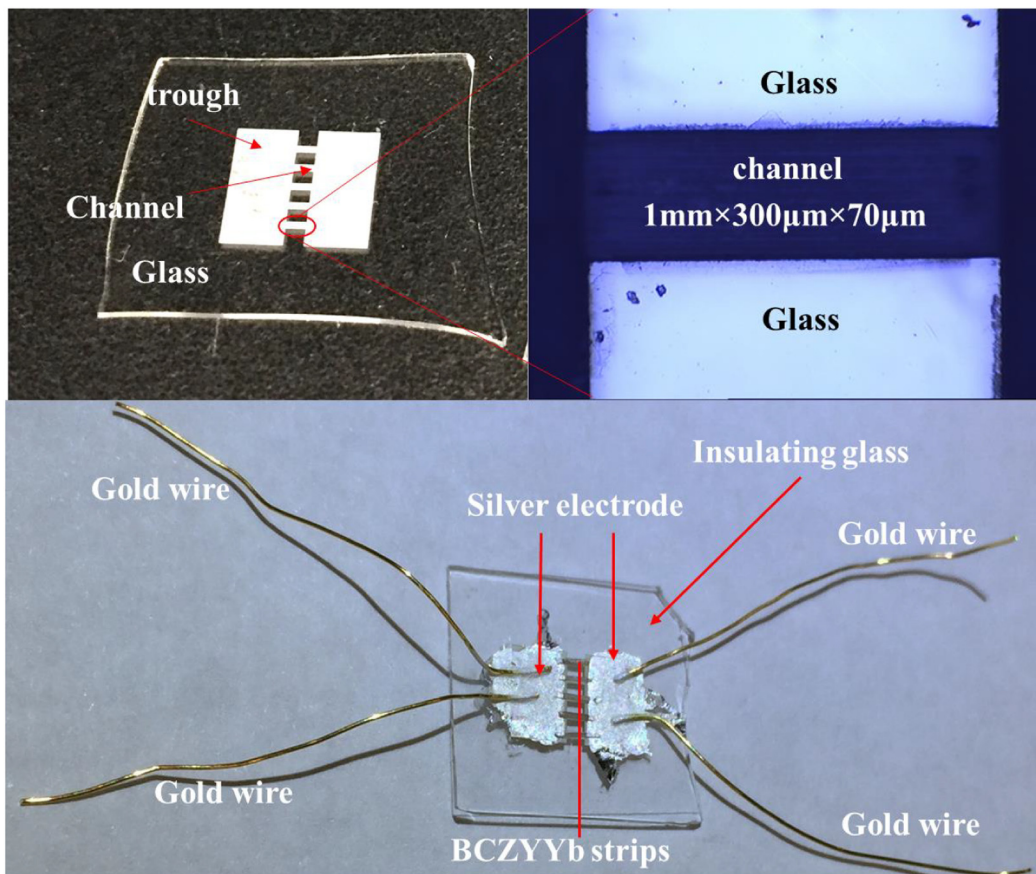
Fig. 2. Five BCZYYb strips after the removal of the porous edges were assembled into five glass channels. The two bigger troughs were designed to connect the channel ends for introducing silver electrodes. The design provided large cross section area and enough mechanical strength for measuring conductivity using electrochemical impedance spectroscopy under different conditions.
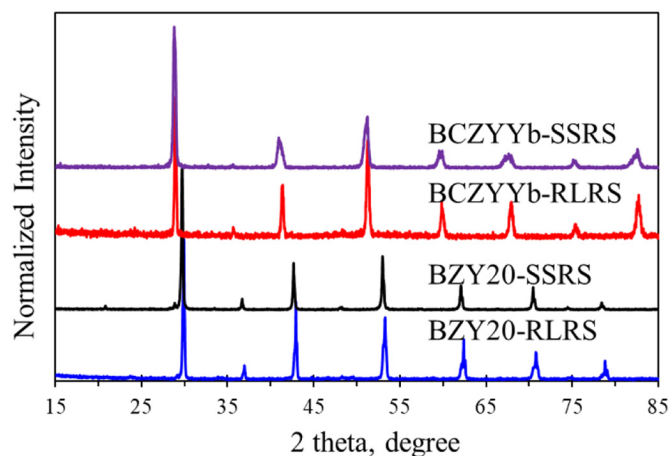
Fig. 3. XRD patterns of the protonic ceramic strips fabricated by rapid laser reactive sintering technology (< 10 s), comparing with the protonic ceramic pellets fabricated by solid state reactive sintering (12 h at 1400–1500 °C). The XRD samples were fine powders ground from respective strips and pellets.

dry Ar, wet Ar, or wet 5% H_2 balanced by Ar. After measurement, the cross-section areas of each strip were analyzed by SEM images. The average total cross-section area of $A = 6.13 \times 10^{-4}\ cm^2$ and length of $L = 1\ mm$ were inserted in the equation of $\sigma = L/(RA)$ for calculating the conductivity.

3. Results and discussion

3.1. Crystal structures

The crystal structures of the BCZYYb and BZY20 strips fabricated by RLRS were analyzed by XRD after grinding into fine powders. Fig. 3

shows the normalized XRD patterns of the two samples. For comparison, the XRD patterns for the two corresponding BCZYYb and BZY20 pellets fabricated by SSRS are also included. In this figure, it can be easily seen that the BCZYYb-RLRS strips and BCZYYb-SSRS pellets have identical XRD patterns and long-range crystalline structure which can be indexed to a pure orthorhombic perovskite structure similar to $BaCeO_3$ (JCPDS card no. 22-0074). The peak intensity for BCZYYb-RLRS strips is relatively higher and sharper than those for BCZYYb-SSRS pellets, which probably indicates better crystallinity in the RLRS samples. On the other hand, a comparison of the BZY20-RLRS strips and the BZY20-SSRS pellets showed similar behavior between the SSRS and RLRS processes. The BZY20-RLRS strips and BZY20-SSRS pellets exhibited similar XRD patterns, which can be indexed to a cubic perovskite similar to $BaZrO_3$ (JCPDS card no. 06-0399). However, the crystallinity difference for the BZY20 ceramics is not apparent. Therefore, the RLRS process appears to be incredibly rapid and effective-processing times on the order of seconds can achieve the same crystal structures for BCZYYb and BZY20 ceramics as the state-of-the-art SSRS process, which take ~10 h at temperatures of 1400–1500 °C.

3.2. Geometric configurations

The rapid laser heating has been successfully used to prepare large plastic and metal parts based on the melting and consolidating mechanism. However, the intrinsic large temperature gradient of laser heating made the rapid sintering of ceramics very difficult, which usually resulted in cracks even in a very small area. By combining with SSRS process, which involved in partial liquid phase sintering, the thermal stress was released in some degree. Fig. 4 shows that, using conducting oxides of $BaCe_{0.7}Zr_{0.1}Y_{0.1}Yb_{0.1}O_{3-\delta}$ (BCZYYb) and $BaZr_{0.8}Y_{0.2}O_{3-\delta}$ (BZY20) as case study, the crack-free protonic ceramic parts of straight strips (~10 mm in length, ~1 mm in width, and 30–200 μm in thickness) (Fig. 4a), spiral strips (~200 mm in length, ~1 mm in width, and 30–200 μm in thickness) (Fig. 4c), and squared
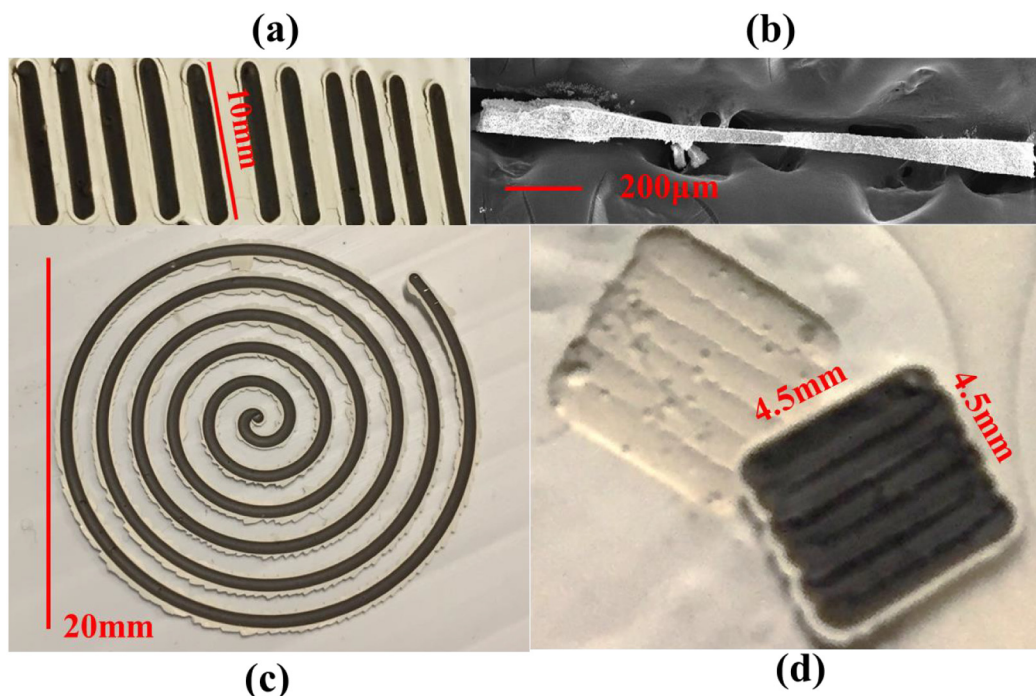

Fig. 4. Images of protonic ceramics BCZYYb and BZY20 after RLRS by a CO_2 laser with maximum power of 20 W. (a) Photo of multiple strips (power 2.8 W, speed 1 mm/s, spacing 0.8 mm, spot size 1.2 mm (20 mm defocus), paste thickness 100 μm, and energy density 2.333 J/mm²). (b) Low magnification micrograph of the strip cross-section (power 7 W, speed 1 mm/s, spot size 1.2 mm (20 mm defocus) paste thickness 100 μm, and energy density 5.833 J/mm²). (c) Photo of spiral BZY20 strip (power 2.8 W, speed 1 mm/s, spacing 0.8 mm, spot size 1.2 mm (20 mm defocus), paste thickness 100 μm, and energy density 2.333 J/mm²). (d) Photo of the squared thin film (power 2.8 W, speed 1 mm/s, spot size 1.2 mm (20 mm defocus), paste thickness 10 mm, and energy density 2.333 J/mm²).
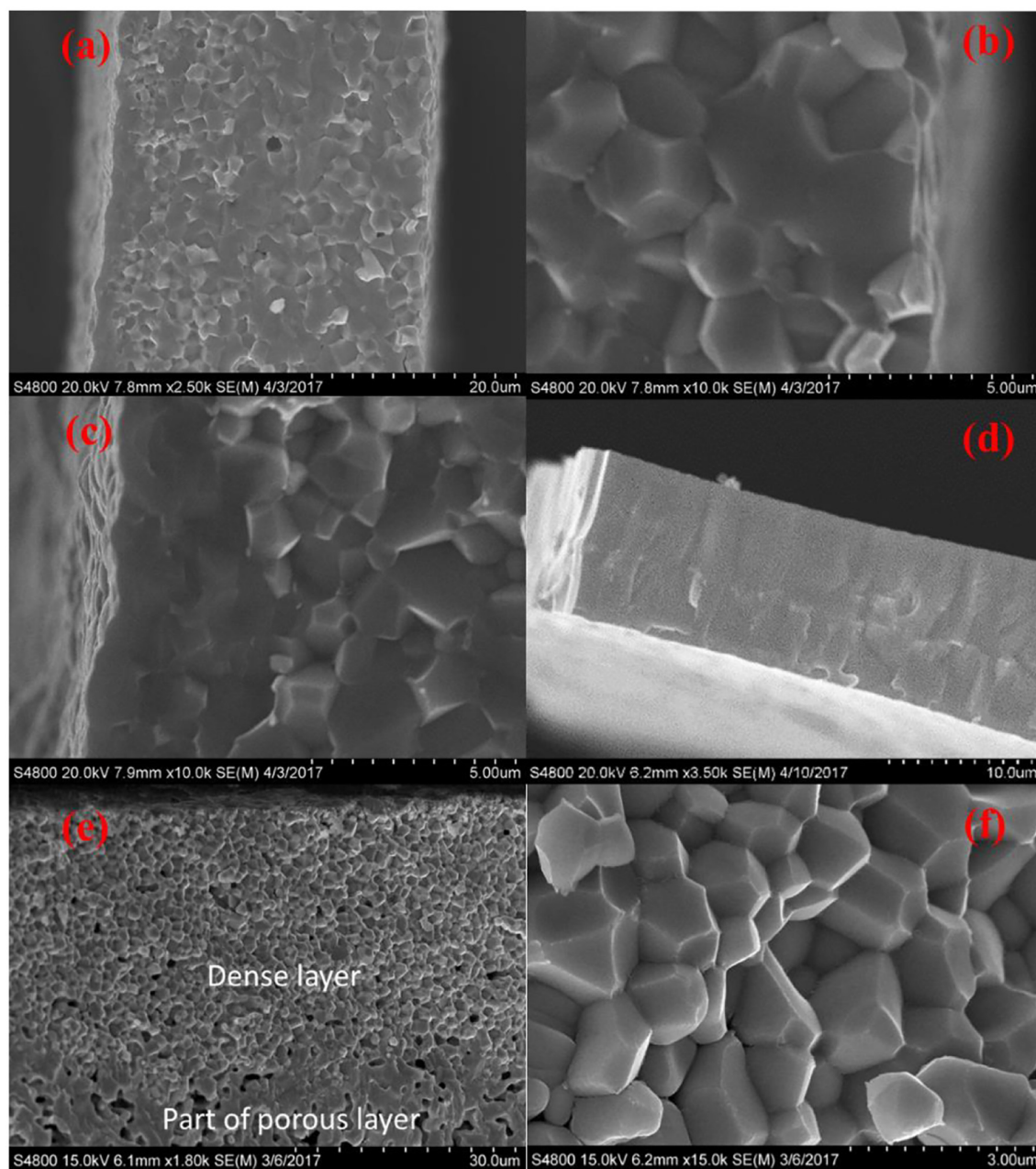
Fig. 5. (a) Dense cross-section of the strip center. (b) Strip cross section near to top surface contacted with a laser beam. (c) Strip cross section near to the bottom surface far from the laser beam. (a), (b), and (c) has the same RLRS conditions (power 2.8 W, speed 1 mm/s, spacing 0.8 mm, spot size 1.2 mm (20 mm defocus), paste thickness 100 μm, and energy density 2.333 J/mm^2). (d) strip cross-section without clear grain boundary (power 5.6 W, speed 0.4 mm/s, spot size 1.2 mm (20 mm defocus), paste thickness 150 μm, and energy density 11.667 J/mm^2). (e) strip cross-section with a dense layer on porous layer (power 20 W, speed 0.8 mm/s, spot size 1.6 mm (60 mm defocus), paste thickness 10 mm, and energy density 15.625 J/mm^2). (f) high magnification micrograph of dense layer in (e) (RLRS conditions are same as (e)).

films (~4.5 mm in both length and width and 30–200 μm in thickness) (Fig. 4d) were successfully fabricated by RLRS method. Fig. 4b provides a low-magnification SEM micrograph of the cross-section for one representative BCZYYb strip. It is clear that there are no cracks existing in the observed cross-section region. The strip thickness varies in the range of 30–200 μm corresponding to the different relative densities. The thickness at the center is thinner than the two edges, which is consistent with the Gaussian distribution of laser power during laser scanning.

3.3. Microstructures

It has been extensively reported that the microstructures of the protonic ceramics significantly affected the performance of the protonic ceramic energy devices [40–42]. For example, the PCFCs usually need the large-grained fully dense protonic ceramic films for electrolytes and the highly porous nanostructures for electrodes. It is evident that two remarkably different firing conditions should be used to obtain the hierarchical electrolyte and electrode layers selectively. Therefore, the capability of engineering microstructures for protonic ceramics is one of the most important factors for evaluating the new fabrication techniques for protonic ceramics.
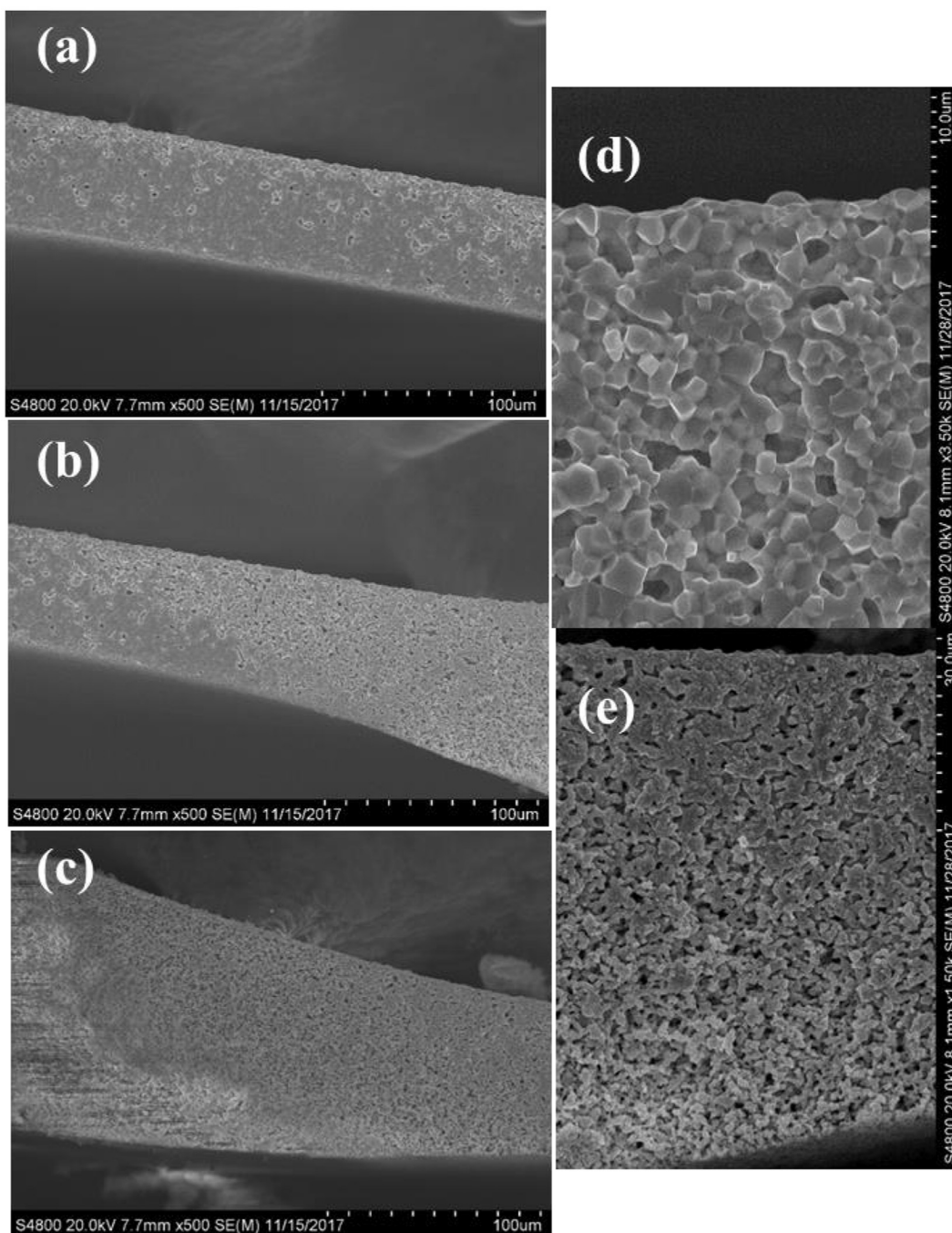
Fig. 6. Microstructures of BCZYYb strips with dense center and two porous edges. (a) dense center, (b) right porous edge, (c) left porous edge, (d) high magnification dense center, and (e) representative porous edge.

Fig. 5 provides a summary of the microstructures of the protonic ceramics (i.e., BCZYYb) fabricated by RLRS technology by adjusting laser operating conditions and substrates. Fig. 5a shows that the strip center is fully densified with a thickness of ~30 μm. Fig. 5b and c indicate that both top region (contact with a laser beam) and bottom region (contact with the fused silica substrate) show the complete densification and are composed of 1–2 μm crystal grains. Fig. 6a and d show that these dense regions for BCZYYb strips usually have widths around 100–300 μm. The very porous regions can be found when we further moved to the edges direction (Fig. 6b, c, and e). Therefore, using one fast laser scan, we can get a sandwich-structured protonic ceramic strip, which can be potentially used for the fabrication of single-chamber fuel cells and micro electrochemical sensors. Fig. 5d shows a cross-section of a BCZYYb strip center region sintered by a higher energy density, which allows the removal of the grain boundary because of the partial liquid phase sintering. We are still optimizing this grain boundary-free fabrication and hope to get a significant improvement on the conductivities. Furthermore, by RLRS thick green layers on alumina substrates, we have prepared free-standing half-cell layers, which consist of thin dense layer ~15–50 μm and a porous layer ~100–200 μm. The representative SEM micrographs of Figs. 5e, f, and 7 indicate that the BCZYYb strips composed of a 35 μm fully densified layer with grain size ~1–2 μm and a ~100 μm porous substrate can be easily fabricated. These half-cell layers are much easier to be used for the fabrication of micro fuel cells, electrolyzers, or electrochemical sensors.
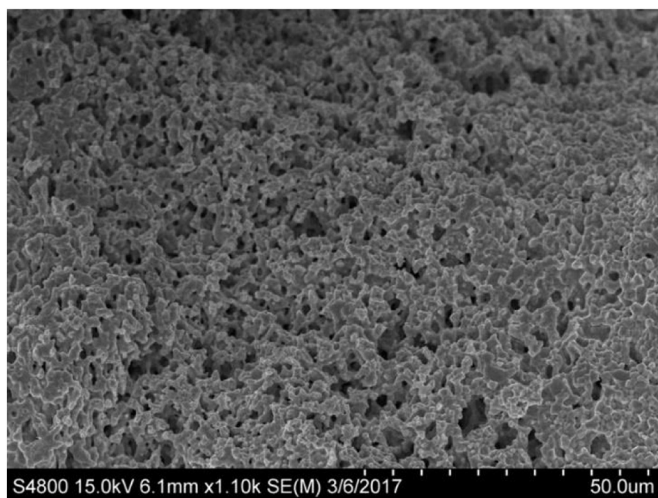
Fig. 7. High magnification porous bottom region of thick BCZYYb layer by RLRS.

Based on the above results, it can be successfully concluded that we can easily achieve BCZYYb protonic ceramic strips with well-engineered microstructures using RLRS processing. BZY20 is another prototypical proton conducting oxide, which is more promising because of the long-term stability [5]. However, BZY20 is difficult to fully densify and achieve large grains because of its high refractory nature. Our RLRS experiments indicate that the BZY20 strips with similar microstructures as BCZYYb strips can also be achieved using the same RLRS technology as shown in Fig. 1. For example, Fig. 4c shows that the BZY20 spiral strips with relatively large dimension were fabricated successfully by RLRS method. Fig. 8a shows that the representative BZY20 strips are fully densified and the thickness is ~20–40 μm. The high magnification SEM micrograph, Fig. 8b, shows well intergrowth between grains because of the involvement of the partial liquid phase sintering.

3.4. Conductivities

The level of proton conductivity is one of the most important properties for evaluating the performance of protonic ceramics fabricated by different methods. Here, the proton conductivity for the BCZYYb strips after removing the porous edges and assembling into the five-strip symmetrical samples (Fig. 2) was analyzed by electrochemical impedance spectroscopy (EIS) at different conditions. Fig. 9 provides a typical EIS Nyquist plot for the measurement under the atmosphere of

5% H_2 balanced by Ar, which shows high-frequency arc and low-frequency arc in the whole temperature range of 300–700 °C. The high-frequency arc goes through the origin, which can be ascribed to the electrolyte contribution. The separation of grain bulk and grain boundary contributions was not observed even at low temperature of 300 °C, which is consistent with most of the other SSRS BCZYYb pellet samples [34]. The low-frequency arc can be ascribed to the electrode kinetics, which gradually evolves to almost straight line (pure constant phase element (CPE)) from the full arc (resistance R and CPE in parallel), corresponding to the gradual decrease in electrode kinetics with the decreasing temperature. The similar EIS Nyquist plots for BCZYYb samples were also observed under both dry Ar and wet Ar atmospheres at the same temperature range, which can be explained in the same way. Therefore, based on the high-frequency arcs, we obtained the total conductivities for the BCZYYb five-strip sample at 300–700 °C under wet 5% H_2 balanced by Ar, wet Ar, and dry Ar atmospheres, which is shown in Fig. 10. It is not surprising that the wet reducing atmosphere (wet 5% H_2 balanced by Ar) shows the highest total conductivities since this atmosphere allows the formation of highest proton concentration in the BCZYYb structure. The existence of large amount of steam in the wet Ar atmosphere also allows the formation of high proton concentration because of the hydration reaction between water and oxygen vacancy and lattice oxygen in the BCZYYb structure. However, the dry Ar only allows the existence of very low concentration of protons because of the extremely low H_2 and H_2O concentration in the dry Ar[1]. The primary charge carriers in BCZYYb under dry Ar atmosphere should be oxygen vacancy and electron-hole. Since the dry Ar, in fact, is also the most oxidizing atmosphere, the corresponding ionic defect concentration (oxygen vacancy) should be the lowest. According to the Arrhenius equation ($\sigma = \sigma_0 \exp(-E_a/RT)$), the activation energies for the total conductivities under wet atmospheres were calculated to be 0.441 ± 0.008 eV and 0.457 ± 0.007 eV for wet 5% H_2 and wet Ar respectively. It is very clear that activation energies in wet atmospheres are close and are similar as the common value reported for proton conduction in BCZYYb and other protonic ceramics [1,7,34]. However, the activation energy under dry Ar can be split into two ranges. At lower temperature 300–500 °C, the activation energy of 0.343 ± 0.005 eV was obtained, which indicates that the electron-hole contribution might play a significant role for transport process in the dry and relatively oxidizing atmosphere [34]. At higher temperature range 500–700 °C, the high activation energy of 0.689 ± 0.020 eV was obtained, which can be ascribed to the oxygen vacancy transport process [1].

In general, we conclude that the BCZYYb dense strips fabricated by RLRS method show promising proton conductivity under wet reducing atmospheres. However, this preliminary proton conductivity is still a
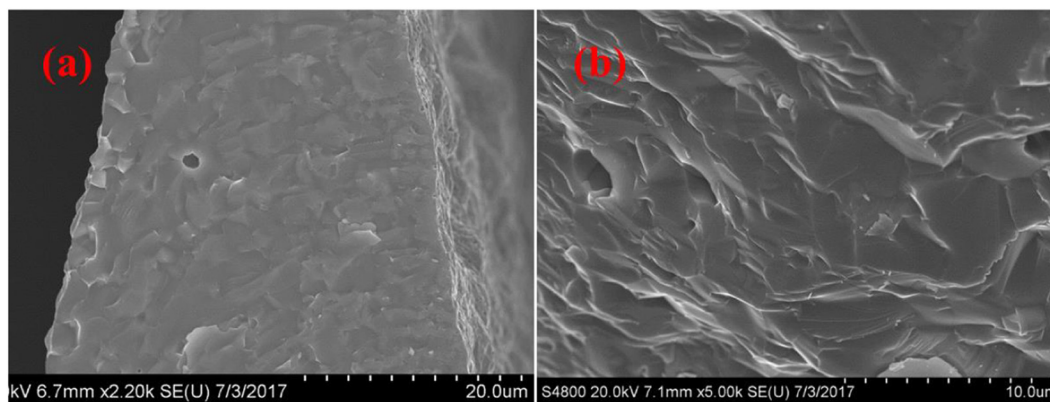

Fig. 8. Representative microstructures of BZY20 strips fabricated by RLRS. (a) Low magnification image showing the thickness of sintered region (power 7 W, speed 1 mm/s, spot size 1.2 mm (20 mm defocus), paste thickness 150 μm, and energy density 5.833 J/mm²). (b) High magnification image showing the grain boundaries are not clear (power 8 W, speed 0.4 mm/s, spot size 1.2 mm (20 mm defocus), paste thickness 150 μm, and energy density 16.667 J/mm²).
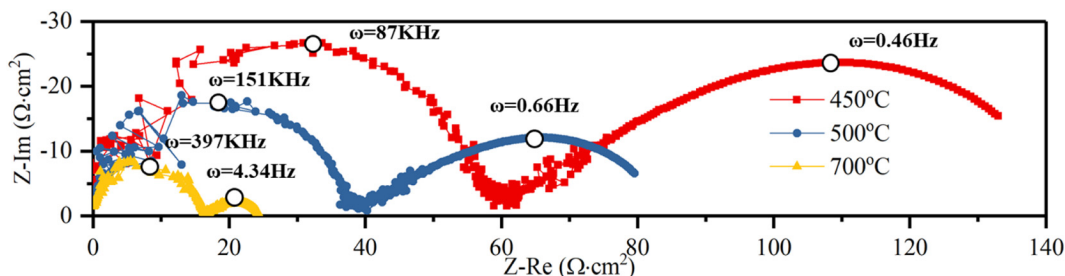
Fig. 9. Nyquist plot for electrochemical impedance spectroscopy for BCZYYb sample under wet 5% H$_2$ balanced by Ar at different temperatures.
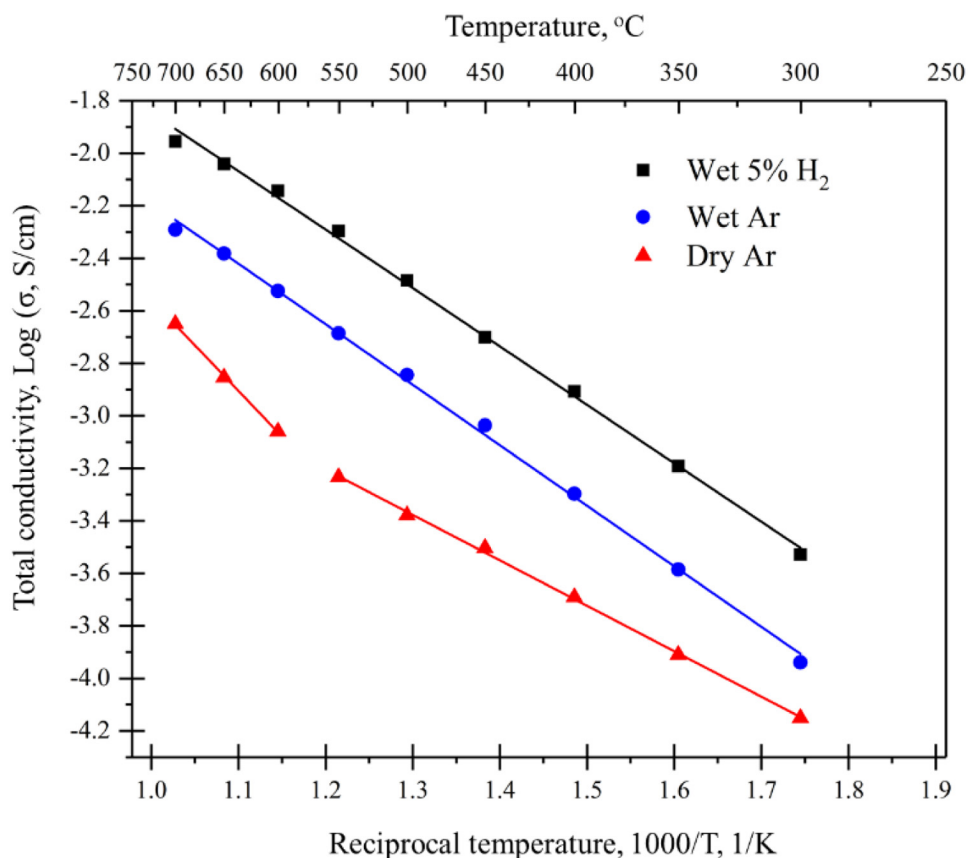

Fig. 10. Total in-plane conductivities of five-strip dense BCZYYb samples measured by EIS at 300–700 °C under wet 5% H$_2$ balanced by Ar, wet Ar, and dry Ar. The wet atmosphere was obtained by flowing through room temperature bubbler.

little lower than that obtained from the corresponding BCZYYb pellets obtained by SSRS technique [7,43]. This relatively low conductivity can be ascribed the high grain boundary density in the lateral direction because of the columnar microstructure of the strips. In our continuous work, we are devoting our effort to study and adjust the potentially spatially different composition of the protonic ceramic strips to eliminate the effect of the possible composition discrepancy. We will also try to measure the strips in different directions (out-of-plane), to check for anisotropic effects to the printing process and due to the high length to cross section ratio made the resistance so high that the big error might be introduced.

4. Conclusions

In conclusion, the newly developed RLRS method was demonstrated as a new, highly effective method to fabricate protonic ceramics with well-controlled microstructures in single firing step from inexpensive carbonates and oxides. The fully dense large-grained, highly porous, porous/dense/porous sandwiched, and dense/porous half-cell

microstructures were successfully fabricated. The electrochemical impedance measurement of the fully dense strips showed promising protonic conductivities. The new RLRS method demonstrated the feasibility and promise of the rapid additive manufacturing of hierarchical ceramic energy devices.

References

[1] K.D. Kreuer, Annu. Rev. Mater. Res. 33 (2003) 333.

[2] P. Babilo, T. Uda, S.M. Haile, J. Mater. Res. 22 (2007) 1322.
[3] N. Kochetova, I. Animitsa, D. Medvedev, A. Demin, P. Tsiakaras, RSC Adv. 6 (2016) 73222.
[4] Y. Yamazaki, R. Hernandez-Sanchez, S.M. Haile, Chem. Mater. 21 (2009) 2755.
[5] C. Duan, J. Tong, M. Shang, S. Nikodemski, M. Sanders, S. Ricote, A. Almansoori, R. O'Hayre, Science 349 (2015) 1321.
[6] M. Shang, J. Tong, R. O'Hayre, RSC Adv. 3 (2013) 15769.
[7] L. Yang, S. Wang, K. Blinn, M. Liu, Z. Liu, Z. Cheng, M. Liu, Science 326 (2009) 126.
[8] B. Hua, N. Yan, M. Li, Y.F. Sun, Y.Q. Zhang, J. Li, T. Etsell, P. Sarkar, J.L. Luo, Adv. Mater. 28 (2016) 8922.
[9] Lei Bi, Samir Boulfrad, Enrico Traversa, Chem. Soc. Rev. 43 (2014) 8255.
[10] M. Dumortier, J. Sanchez, M. Keddam, O. Lacroix, Int. J. Hydrog. Energy 38 (2013) 2610.
[11] V. Garagounis, A. Kyriakou, E. Skodra, Vasileiou, M. Stoukides, Front. Energy Res. 2 (2014) 1.
[12] C.Y. Yoo, J.H. Park, K. Kim, J.I. Han, E.Y. Jeong, C.H. Jeong, H.C. Yoon, J.N. Kim, ACS Sustain. Chem. Eng. 5 (2017) 7972.
[13] H. Borland, L. Llivina, S. Colominas, J. Abellà, Fusion Engineering and Design 88 (2013) 2431.
[14] H. Farahani, R. Wagiran, M.N. Hamidon, Sensors 14 (2014) 7881.
[15] W.G. Coors, Solid State Ionics 178 (2007) 481.
[16] M.D. Sanders, R.P. O'Hayre, J. Membr. Sci. 376 (2011) 96.
[17] T. Norby, Y. Larring, Solid State Ionics 136-137 (2000) 139.
[18] J.W. Phair, S.P.S. Badwal, Ionics 12 (2006) 103.
[19] E. Rebollo, C. Mortalò, S. Escolástico, S. Boldrini, S. Barison, J.M. Serra, M. Fabrizio, Energy Environ. Sci. 8 (2015) 3675.
[20] H.G. Bohn, T. Schober, J. Am. Ceram. Soc. 83 (2000) 768.
[21] F. Iguchi, T. Yamda, N. Sata, T. Tsurui, H. Yugami, Solid State Ionics 177 (2006) 2381.
[22] S.B.C. Duval, P. Holtappels, U.F. Vogt, E. Pomjakushina, K. Conder, Solid State Ionics 178 (2007) 1437.
[23] A. Sin, B.E. Montaser, P. Odier, J. Am. Ceram. Soc. 85 (2002) 1928.
[24] G. Taglieri, M. Tersigni, P.L. Villa, C. Mondelli, Int. J. Inorg. Mater. 1 (1999) 103.
[25] P. Balilo, S.M. Haile, J. Am. Ceram. Soc. 88 (2005) 2362.
[26] S.W. Tao, J.T.S. Irvine, J. Solid State Chem. 180 (2007) 3493.
[27] A.M. Azad, S. Subramaniam, T.W. Dung, J. Alloys Compd. 334 (2002) 118.
[28] J. Tong, D. Clark, M. Hoban, R. O'Hayre, Solid State Ionics 181 (2010) 496.
[29] J. Tong, D. Clark, L. Bernau, M. Sanders, R. O'Hayre, J. Mater. Chem. 20 (2010) 6333.
[30] J. Tong, D. Clark, L. Bernau, A. Subramaniyan, R. O'Hayre, Solid State Ionics 181 (2010) 1486.
[31] S. Nikodemski, J. Tong, C. Duan, R. O'Hayre, Solid State Ionics 294 (2016) 37.
[32] S.H. Morejudo, R. Zanón, S. Escolástico, I. Yuste-Tirados, H. Malerød-Fjeld, P.K. Vestre, W.G. Coors, A. Martínez, T. Norby, J.M. Serra, C. Kjølseth, Science 353 (2016) 563.
[33] B.P. Conner, G.P. Manogharan, A.N. Martof, L.M. Rodomsky, C.M. Rodomsky, D.C. Jordan, J.W. Limperos, Additive Manufacturing 1-4 (2014) 64.
[34] S.H. Huang, P. Liu, A. Mokasdar, L. Hou, Int. J. Adv. Manuf. Technol. 67 (2013) 1191.
[35] J. Lei, A.A. Trofimov, J. Chen, Z. Chen, Y. Hong, L. Yuan, W. Zhu, Q. Zhang, L.G. Jacobsohn, P. Peng, R.K. Bordia, H. Xiao, Opt. Mater. 68 (2017) 63.
[36] S. Nikodemski, J. Tong, R. O'Hayre, Solid State Ionics 253 (2013) 201.
[37] J. Tong, M. Shang, R. O'Hayre, US Patent, Publication date, 02/04/2016, Application number 14/621091.
[38] S. Nikodemski, J. Tong, C. Duan, R. O'Hayre, Solid State Ionics 294 (2016) 37.
[39] A. Evans, A. Bieberle-Hütter, J.L.M. Rupp, L.J. Gauckler, J. Power Sources 194 (2009) 119.
[40] P. Babilo, T. Uda, S.M. Haile, J. Mater. Res. 22 (2007) 1322.
[41] D. Han, N. Hatada, T. Uda, J. Electrochem. Soc. 163 (2016) F470.
[42] L. Malavasi, C.A.J. Fisher, M.S. Islam, Chem. Soc. Rev. 39 (2010) 4370.
[43] D. Clark, J. Tong, A. Morrissey, A. Almansoori, I. Reimanis, R. O'Hayre, Phys. Chem. Chem. Phys. 16 (2014) 5076.